ChemEurJ

Research Article
doi.org/10.1002/chem.202501682

Chemistry Europe
European Chemical Societies Publishing

www.chemeurj.org

VIP *Very Important Paper*

Zinc(II) Monomeric, Dimeric, and Trimeric Photosensitizers with Microsecond-Lived Intra-ligand Charge Transfer Excited States Investigated through Time-Resolved Optical and X-Ray Spectroscopy

Maxime Sauvan,[a] Lucia Velasco,[a] Leonel Llanos Silva,[b] Asterios Charisiadis,[a] Pedro Levín,[b] Saül Garcia-Orrit,[c] Victor Vega-Mayoral,[c] Juan Cabanillas-Gonzalez,[c] Xiaoyi Zhang,[d] Daniel Aravena,*[b] Luis Lemus,*[b] and Dooshaye Moonshiram*[a]

Zn^{II} photosensitizers relative to Cu^{I} complexes have received less attention due to their energetically higher metal-to-ligand charge transfer states. Three Zn^{II} complexes, namely a Monomer, a bimetallic helicate, and a trimetallic helicate, bearing phenanthroline ligands are hereby studied through time-resolved X-ray absorption (tr-XAS) and femto-microsecond optical transient absorption spectroscopy (OTA). The formation of intraligand singlet charge transfer (^{1}ILCT) excited states is achieved within femtoseconds, followed by intersystem crossing (ISC) in nanoseconds to generate microsecond-lived triplet (^{3}ILCT) states. Femtosecond OTA shows that the ^{1}ILCT states in the Monomer, Dimer, and Trimer occur within 235 fs, 683 fs, and 730 fs, respectively, while nano-microsecond OTA and tr-XAS show their ^{3}ILCT states to decay within 1.00 µs, 1.48 µs, and 1.51 µs. The ISC from the ^{1}ILCT to the ^{3}ILCT state for the Trimer is 42.8 ns compared to the Monomer and Dimer with ISC rates of less than 13 ns. These differences arise due to the stabilization by π-π and CH-π non-covalent interactions of the phenanthroline ligands. The dihedral and torsional angles indicate stronger ligand strains in the excited states of the Dimer and Trimer versus the Monomer. DFT calculations for the electrochemical oxidation potentials further highlight their capability in inducing photoredox processes.

1. Introduction

The search for sustainable ways to store and distribute energy is one of the most urgent scientific challenges in view of the rapid depletion of fossil fuels, environmental pollution, and resulting climate emergency.[1] Means of storing energy from the sun through fuel-forming reactions inspired by natural photosynthesis,[2] such as the light-induced splitting of water into hydrogen or the water reduction of CO_2 to generate liquid organic fuels, are both attractive means of minimizing the environmental impact and have successfully led to the design of "sunlight-to-fuel" assemblies.[3] Such arrays consist of a chromophore linked to a multi-electron, multi-proton catalytic module and are capable of absorbing visible light through the light-harvesting unit, and converting it into a chemical potential through charge accumulation processes. Importantly, the charge-separated excited state of such assemblies is critical for their photocatalytic applications; thus, traditionally consisting of expensive, precious, and rare 4d or 5d transition metals such as ruthenium,[4] rhenium,[5] osmium,[6] iridium,[7] and platinum.[8] Systems based on those noble metals are capable of displaying impressive photophysical and electrochemical properties as well as long-lived metal-to ligand charge transfer (MLCT) states whereby an electron is promoted from a metal d orbital to a ligand orbital. The capability of 4d and 5d transition metals to govern a diverse array of photochemical properties has mainly been due to their stronger ligand fields and larger spatial overlap of their d orbitals with relevant ligand orbitals, [9] in comparison to earth-abundant transition metals, which have more contracted 3d orbitals. However, over the course of the past decades, a paradigm shift toward the implementation of transition metal complexes based on Cu,[10–12] Mo,[13] Cr,[14–17] Mn,[18,19] Fe,[20,21] Ni,[22,23] Co,[24] V,[25] and Zn[26] has appeared with the aim of using these economically feasible metals in photochemistry. For

[a] M. Sauvan, L. Velasco, Dr. A. Charisiadis, Dr. D. Moonshiram
Instituto de Ciencia de Materiales de Madrid (ICMM-CSIC), Sor Juana Inés de la Cruz, 3, Madrid 8049, Spain
E-mail: dooshaye.moonshiram@csic.es

[b] Dr. L. Llanos Silva, Dr. P. Levín, Dr. D. Aravena, Dr. L. Lemus
Departamento de Química de los Materiales, Universidad de Santiago de Chile, Santiago, Chile
E-mail: daniel.aravena.p@usach.cl
luis.lemus@usach.cl

[c] Dr. S. Garcia-Orrit, Dr. V. Vega-Mayoral, Dr. J. Cabanillas-Gonzalez
Instituto Madrileño de Estudios Avanzados en Nanociencia (IMDEA Nanociencia), Calle Faraday, 9, Madrid 28049, Spain

[d] Dr. X. Zhang
X-ray Science Division, Argonne National Laboratory, 9700 S. Cass Avenue, Lemont IL, USA

Supporting information for this article is available on the WWW under https://doi.org/10.1002/chem.202501682

instance, heteroleptic diphosphine-diimine Cu^{I} complexes with diphosphine and diimine ligands[10] together with Cu Dimeric helicate[11] complexes with 1,2-bis(9-methyl-1,10-phenanthrolin-2-yl)ethane ligands, have shown triplet ^{3}MLCT excited states with nano-microsecond lifetimes. Additional examples concern complexes of Mo^{0}, Cr^{0} with diisocyanide ligands and pyrene units,[15] Mn^{I} with chelate isocyanide ligands,[18] Fe^{III} with *N*-heterocyclic carbenes bearing two cyclometalating aryl units[20] as well as Ni^{II} complexes with N-heterocyclic carbenes[22] and carbazoylyl cyclometalating tetradentate ligands[23] that have all displayed nano-submicrosecond ^{3}MLCT excited state deactivation pathways. Those findings are crucial for the development of first-row photoactive complexes. Microsecond long-lived ligand-ligand charge transfer (LLCT) excited states have further been exhibited by Cu^{I} complexes[12] with combined donor and acceptor ligands based on cyclic monoamidocarbene groups with carbazolate ligands. Moreover, Fe^{III} with N-heterocyclic carbene tris-bidentate ligands, [21] mono-anionic facial *tris*-carbene ligands[27] , *N*-heterocyclic carbenes with two cyclometalating aryl units[20] and Co^{III} complexes with six-membered chelate ligands[28] containing the strongly σ-donating pyrimidine moiety have shown nanosecond ligand-metal charge transfer (LMCT) excited states. Lastly, micro-millisecond metal-centered (MC) excited states have also been recorded for systems based on V^{III} with N,N′-dimethyl-N,N′-dipyridine ligands,[25] Cr^{III} with tris(pyrid-2-yl)ethane[16] and heteroleptic polypyridyl[17] ligands, bis(tris(carbene)borate) Mn^{IV} solid-state complexes[19] and hexacarbene-Co^{III} complexes. [24]

The photochemical reactivities of these earth-abundant systems have been achieved mainly through the formation of triplet excited states that can participate in photoinduced electron transfer reactions. In this respect, the exploration of Zn^{II}-based complexes for photophysical and photochemical applications has been less common. Zn^{II} complexes versus Cu^{I} have high oxidation potentials, which prohibit the formation of ^{3}MLCT or ^{3}MC states.[29] For this reason, Zn^{II} complexes have mainly been shown to exhibit ligand-based fluorescence[26] rather than excited states with triplet character that could be involved in energy transfer catalysis or photoinduced electron transfer as previously illustrated.[30]

Phenanthroline ligands are particularly appealing due to their energy-donating abilities and rigid scaffolds, stabilizing the excited states of their complexes, and behaving as building blocks[32] for the formation of multinuclear complexes with rigid coordination environments. It is important to remark that the study of photoactive Zn^{II} complexes has been restricted to mononuclear structures due to the unusual aggregation or disaggregation of multinuclear Zn^{II} species[33] in solution. The implementation of phenanthroline ligands thus enables the study of novel redox-active structures with π-extended frameworks[34] and allows us to study stable photoactive Zn^{II} complexes that are not only monomeric in nature.

Previously, we studied the photochemical properties of a set of phenanthrolinic Zn^{II} complexes capable of inducing photoredox processes.[31] In particular, a mononuclear complex, a linear bimetallic helicate, and a circular trimetallic helicate (Scheme 1), were able to oxidize 2-propanol and reduce methyl viologen

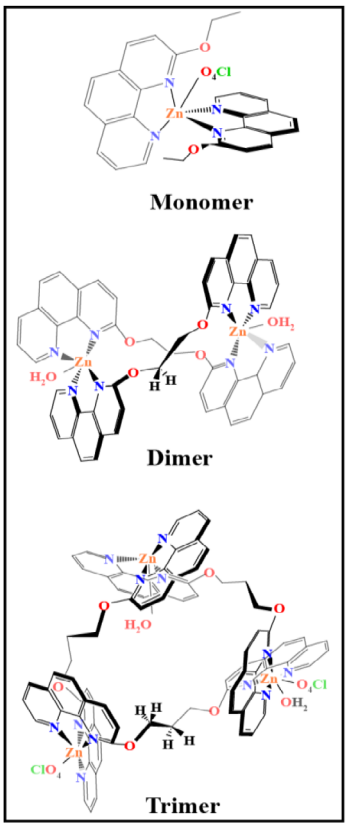

Scheme 1. Zn-based photosensitizers investigated in this study.[31].

upon excitation at their IL bands. This property can only be conceived if the initial excited states lead to charge transfer states, where the participation of d orbitals from Zn^{II} is unlikely. In this scenario, the involvement of ILCT or LLCT states could explain the photoreactivity observed, which was also dependent on the supramolecular topologies of the complexes.

Accordingly, the conformation of the linear bimetallic helicate is stabilized by π-π stacking interactions, while the circular trimetallic helicate is supported by CH-π interactions. These non-covalent forces define aromatic surfaces that can interact with the substrate, either in the ground or the excited states, in addition to imparting higher structural constraints as the nuclearity of the complexes increases.

Aiming to elucidate the nature and dynamics of the reactive excited states of the three Zn^{II} complexes, femto-microsecond optical transient absorption spectroscopy (OTA) coupled with picosecond time-resolved X-ray absorption spectroscopy (tr-XAS) and time-dependent density functional theoretical calculations (TD-DFT) were applied.[31] It is important to remark that both OTA and tr-XAS have played a pivotal role in providing insights into the dynamics and real-time visualizations of photoinduced processes. Therefore, the interrelated employment of those two techniques has reshaped our approach to the study of ultrafast processes at an atomic and molecular level.[35] By probing photocatalytic systems on a pico-microsecond timescale, tr-XAS has delivered real-time snapshots of molecular dynamics, allowing us to follow reactions and underlying structural configurations[11,35–37] with remarkable precision.

Combined experimental and theoretical results enabled us to reveal the formation of femtosecond-lived singlet excited states for all three complexes followed by an intersystem crossing to generate microsecond long-lived intra-ligand (^{3}ILCT) triplet excited states. These are important features toward applications such as energy transfer and photoredox catalysis for solar energy conversion.

2. Results and Discussion

2.1. Electronic and Structural Nature of the Monomer, Dimer, and Trimer in Solution

Steady-state X-ray absorption near edge structure (XANES) and extended X-ray absorption fine structure (EXAFS) analysis (Figure 1) are first carried out on the three Zn photosensitizers in 100% acetonitrile to guarantee compatibility with our previous results. [31] A polar solvent was hereby further chosen due to the more favored formation of an intramolecular charge-separated state coupled with an increase in the quantum yield of the triplet's excited state as previously shown. [38]

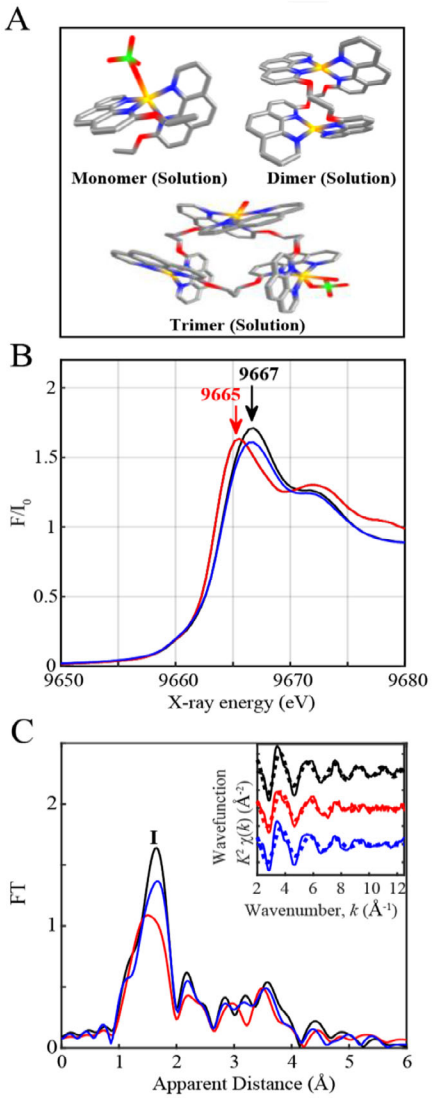

Figure 1. A) DFT-optimized structures of the Zn-based photosensitizers in solution. B) Normalized Zn K-edge XANES and C) Fourier transforms of k^2-weighted EXAFS for the Monomeric (black), Dimeric (red), and Trimeric (blue) Zn complexes. **Inset**. $k^2[\chi(k)]$-weighted traces as a function of k, the photoelectron wavevector (solid lines), and fitted (dashed lines) of the Zn complexes. Experimental spectra were calculated for k values of 2–12.5 Å^{-1}.

The Zn K-edge XANES spectra of the Monomer, Dimer, and Trimer show a rising edge from 9660 to ~9667 eV with the Dimer exhibiting a negative energy shift of -0.55 eV at a normalized fluorescence of 0.8 compared to the Monomer and Trimer (Figure 1B). The Monomer and Trimer further display a principal maximum or white line, attributed to the sharp rise in the X-ray absorption spectrum at 9667 eV, whereas the Dimer shows this feature at 9665 eV (Figure 1B). The observed changes in the XANES spectra indicate variations in the coordination spheres and local symmetries of each Zn-complex as previously indicated through the X-ray diffraction analysis[31] (XRD, Table S1). Importantly, the observed energy shift of 0.55 eV from 9663.05 eV for the Dimer to 9663.60 eV for both the Monomer and Trimer (Figure 1B) denotes that less energy is required to eject a core 1 s electron from the dimeric complex. As elaborated below, this observation is further supported through the structural conformations derived from the EXAFS analysis.

A prominent peak (**Peak I**) is observed in the Fourier-transformed EXAFS spectra of the Monomer, Dimer, and Trimer corresponding to the averaged Zn-N/O bond distances (Figure 1C). The EXAFS fits for the extraction of the actual bond distances of all three complexes are shown in Figure 1C inset, Figure S1 and Table S2. Analysis of the EXAFS spectrum of the monomer reveals 4 Zn-N bonds with an average distance of 2.15 Å (Table S2, Fit 1) and an improvement of the overall fit quality upon addition of 1 versus 2 perchlorate molecules at 2.29 Å (Table S2, Fits 2 versus 3). DFT optimizations on the Zn complexes were further carried out using the r2SCAN density functional[39] with accounted solvent effects of acetonitrile by means of the SMD approximation. [40] The average theoretically determined Zn-N and Zn-ClO_4 distances for the monomer in solution are in close agreement with the experimentally determined distances from EXAFS analysis, deviating from them by 0.09 Å and 0.05 Å, respectively (Table 1).

Furthermore, only 1 perchlorate molecule was found to form a loose coordination bond with the Zn metal center from both EXAFS and DFT optimizations conducted in solution (Table 1). This is in contrast with XRD analysis[31] which reveals 2 bonded oxygens of the perchlorate counter anion to the Zn Monomeric center (Scheme 1, Table S2), thus showing a modified structural conformation and expected distortion of the perchlorate counter anion in solution versus in solid state.

EXAFS analysis of the Dimeric complex in solution further shows improvement of the overall fit quality with 4 versus 5 Zn-N/O bond distances at 2.12 Å (Table S2, Fits 4 vs. 5), once more showing the dissociation of the labile water solvent molecules observed in XRD[31] studies (Table S1). The lower coordination geometry of the dimer also explains the negative energy shift observed in its rising edge compared to the Monomer and Trimer and reflects the smaller ionization energy required to eject a core 1 s electron from a 4- versus 5-coordinated geometrical conformation (Scheme 1).[41] By contrast, the Trimer reveals

Table 1. Comparison of structural parameters obtained from EXAFS.

Complexes	EXAFS fits [Å]	DFT Ground State [Å]	DFT Excited State [Å]
Monomer	**Zn-N, 4: 2.15** **Zn-O, 1: 2.29**	Zn-N: 2.061, 2.082, 2.083, 2.091 Zn-ClO_4: 2.356, 2.494 Torsional angle[a]: 71.2° **Zn-N, 4: 2.08** **Zn-O, 1: 2.35**	Zn-N: 2.037, 2.141, 2.005, 2.065 Zn-ClO_4: 2.292, 3.002 Torsional angle:85.4° **Δ Torsional angle: 14.2°** **Zn-N, 4: 2.06** **Zn-O, 1: 2.29**
Dimer	**Zn-N, 4: 2.12**	Zn-N (Center 1): 2.013, 2.014, 2.025, 2.024 Torsional angle: 68.8° Zn-N (Center 2): 2.014, 2.013, 2.024, 2.025 Torsional angle: 68.8° **Zn-N, 4: 2.03** **Avg**. Torsional angle: 68.8°	Zn-N (Center 1): 2.016, 2.010, 2.024, 2.026 Torsional angle: 68.2° Zn-N (Center 2): 2.028, 2.021, 2.030, 1.992 Torsional angle: 67.0° **Zn-N, 4: 2.03** Torsional angle avg.: 67.6° **Δ Avg. Torsional angle: 1.2°**
Trimer	**Zn-N, 4: 2.15** **Zn-O, 1: 2.27**	Zn-N: (Center 1): 2.012, 2.006, 2.036, 2.021 Torsional angle: 72.8° Zn-N: (Center 2): 2.102, 2.021, 2.075, 2.055 Zn- OH_2 (Center 2): 2.312 Torsional angle: 70.4° Zn-N: (Center 3): 2.110, 2.094, 2.106, 2.123 Zn-OH_2 (Center 3): 2.207 Zn- ClO_4 (Center 3): 2.406 Torsional angle: 82.4° **Zn-N,4: 2.07** **Zn-O, 1: 2.26** Avg. Torsional angle: 75.2°	Zn-N: (Center 1): 2.011, 2.030, 1.982, 2.040 Torsional angle:72.7° Zn-N: (Center 2): 2.021, 2.101, 2.055, 2.073 Zn- OH_2 (Center 2): 2.314 Torsional angle: 70.6° Zn-N: (Center 3): 2.111, 2.095, 2.106, 2.122 Zn-OH_2 (Center 3): 2.208 Zn-ClO_4 (Center 3): 2.405 Torsional angle:82.7° **Zn-N,4: 2.07** **Zn-O, 1: 2.26** Torsional angle avg.: 75.3° **Δ Avg. Torsional angle: 0.1°**

[a] Torsional angle between the 2 ligand planes

the best fit quality with 4 averaged Zn-N bond distances at 2.15 Å and 1 elongated Zn-OH_2/ClO_4 bond distance at 2.27 Å (Table S2, Fit 8).

The average theoretically determined Zn-N bond distances for the Dimer and Trimer in solution lie within 0.09 Å and 0.08 Å of the experimentally determined EXAFS distances, respectively (Table 1). Furthermore, the DFT-optimized bond distance for the Zn-ClO_4/OH_2 of the Trimeric complex deviates from its EXAFS-fitted bond distance by 0.03 Å (Table 1). It is important to remark that, similar to the Monomer and Dimer, the Trimer shows elongation of one of the perchlorate counter anions in solution revealing the expected lability of the bonded solvent/counter anions in this family of Zn-based photosensitizers in solution versus solid. The Zn-N bond distances derived from EXAFS analysis also show elongated Zn-N bond distances of 2.15 Å in the Trimer as well as the Monomer versus that of 2.12 Å (Table 1, S2) obtained for the Dimer which agrees with the theoretically observed trends. This confirms the suitability of the theoretical methods to account for the main structural trends in the studied systems. These results are also of relevance for photosensitizers´ studies that are performed in solution and can be extrapolated to a wide range of reported complexes[11,42] of similar structures bearing labile aqua ligands and perchlorate counteranions.

2.2. Elucidation of the ^{1}ILCT and ^{3}ILCT States Through Femto-Microsecond OTA Spectroscopy

The Zn^{II} photosensitizers with a full and closed-shell electronic configuration are known to display electronic states with π-π* character (Figure 2), as d-d metal-centered transitions are not allowed.[31] The UV-Vis absorption spectra of all 3 complexes display an absorption band between 250 and 300 nm with a maximum around 271–277 nm, which is attributed to ligand-centered π-π* transitions as previously reported (Figure 2).[31] Upon light excitation, Zn photosensitizers, where IL excitations play a dominant role[9] initially form the ^{1}ILCT and subsequently undergo an ISC to eventually populate a ^{3}ILCT state.

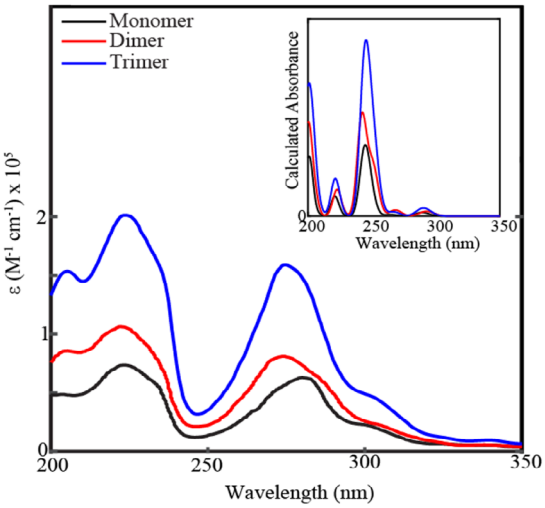

Figure 2. Experimental electronic spectra **Inset**. TD-DFT calculated UV-vis spectra of the Monomer (black), Dimer (red), and Trimer (blue).

To confirm the ILCT nature of the lowest excited states, TD-DFT calculations were carried out using the Tamm-Damcoff approximation[43] and the ωB97X-D functional.[44,45] All complexes presented a similar spectral profile, consistent with UV-vis measurements in acetonitrile (Figure 2 **inset**).[31] Lower energy excitations correspond to ligand-centered π-π* transitions from the phenanthroline groups (see Natural Transition Orbitals for the $S_0 \rightarrow S_1$ transition in Figures S2–S5). As expected, these bands are weak due to the low transition dipole moment associated with these local excitations. Stronger absorption bands appear at higher energy (around 250 nm in calculations), where transitions have a larger charge transfer character.

The formations of the ILCT states of the three photosensitizers were further determined through complementary femto-picosecond OTA (Figures 3, S6) and nano-microsecond OTA (Figures 4, S6) with instrumental response functions (IRF) of 120 fs, and 13 ns, respectively (please see Experimental Section for more details). Upon laser excitation at 258 nm, the Monomer exhibits a broad absorption band between ~480 and 640 nm centered at ~540 nm after around 359 fs (Figure 3B, Figure S6). The Dimer and Trimer in comparison exhibit a broad absorption band centered at ~570 nm and ~560 nm after around 904 fs and 1.17 ps (Figure 3C, Figure S6), respectively.

It is important to remark that the decay lifetimes of the singlet excited states of Zn photosensitizers with phthalocyanine ligands[46] and di(anisyl) amino substituents in a para position of the benzoxazole unit[30] have been known to display lifetimes of 2.9 ns and 5.5 ns, respectively. Thus, given the femtosecond and sub-picosecond lifetimes of these 3 spectral features, they can be assigned to the formation of the singlet excited states ^{1}ILCT. The kinetics for the formation of the ^{1}ILCT were further monitored in the femto-picosecond time scale from 0 ps to 6 ps as shown in Figure 3A through global fit analysis (Figure S7). The ^{1}ILCT excited states for the Monomer, Dimer, and Trimer occur within 235 ± 45 fs, 683 ± 194 fs and 838 ± 174 fs, respectively (Figure 3A, S7).

It is also worth noting that the Dimer is largely stabilized by π-π interactions between the adjacent phenanthroline ligands whereas the addition of the extra methylene substituent in the Trimer gives rise to CH-π noncovalent interactions, which contribute even further to the stabilization of the circular helicate. The difference in the topologies and structural conformations of the three Zn complexes bears a very important effect on the lifetimes of their single excited states, with the Dimer and Trimer showing a ~threefold increase compared to the Monomer.

Nano-microsecond OTA (Figures 4, S6) was further employed to investigate the ISC rate from the ^{1}ILCT to generate the ^{3}ILCT as well as the lifetimes and stabilities of the ^{3}ILCT states. Upon laser excitation at 355 nm, the Monomer illustrates a broad absorption band with two noticeable peaks at 480 and 560 nm (Figure 4B, S6, Table 2), which decrease in intensity from 16 ns to 1.34 µs, whereas the Dimer similarly displays a broad absorption with two peaks at 505 and 570 nm (Figure 4C, S6, Table 2). The Trimer by contrast displays the ^{1}ILCT peak at ~ 560 nm at 40 ns (Figure 4D, Table 2, Figures S6, S8), similar to that observed in Figure 3D and Figure S6, which blue shifts to two peaks at 490 nm and 550 nm from 56 ns to 1.34 µs (Figure 4D, Figure S6). Such broad excited-state absorption features have been observed in the radical anion spectra of Cu photosensitizers with similar phenanthroline ligands.[47] The isobestic points for the conversion of the ^{1}ILCT to ^{3}ILCT states were further shown to occur at ~520 nm, ~530 nm, and ~565 nm for the Monomer, Dimer, and Trimer, respectively (Figure S6).

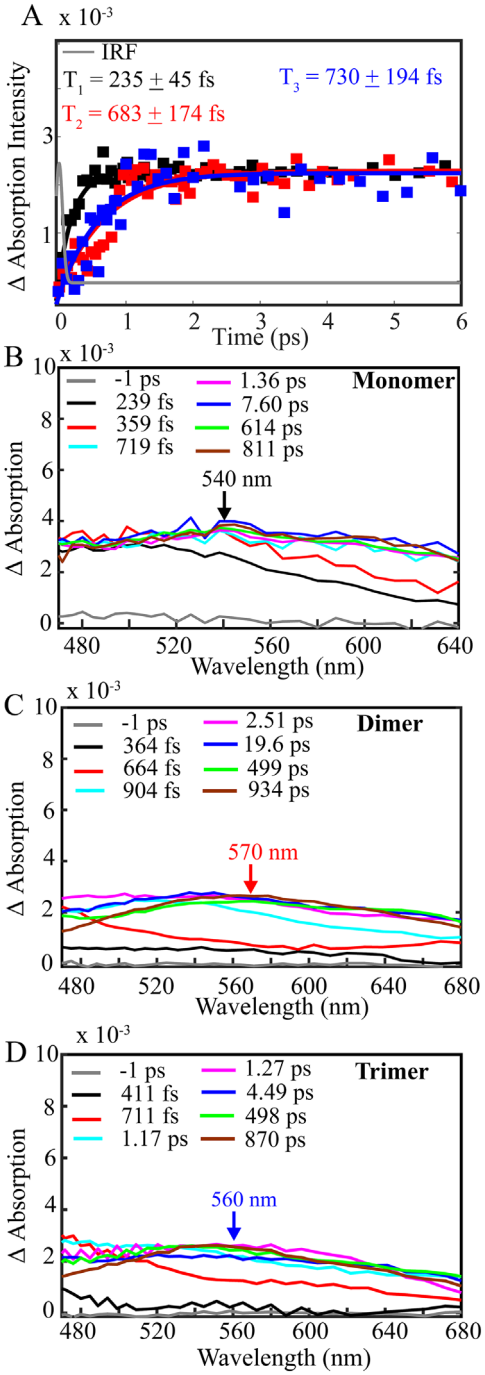

Figure 3. A) Global fit Kinetic decay profiles shown here at 558 nm (Monomer (in black), Dimer (in red), and 580 nm (Trimer (in blue)) after excitation at λ_{exc} = 258 nm illustrating the formation of the singlet excited state with the instrumental response function of 120 fs (shown in gray). OTA spectra of a solution of B) Monomer, C) Dimer D) Trimer dissolved in CH_3CN, with an optical density of 1 at the pump excitation of 258 nm, from 0 to 1 ns.

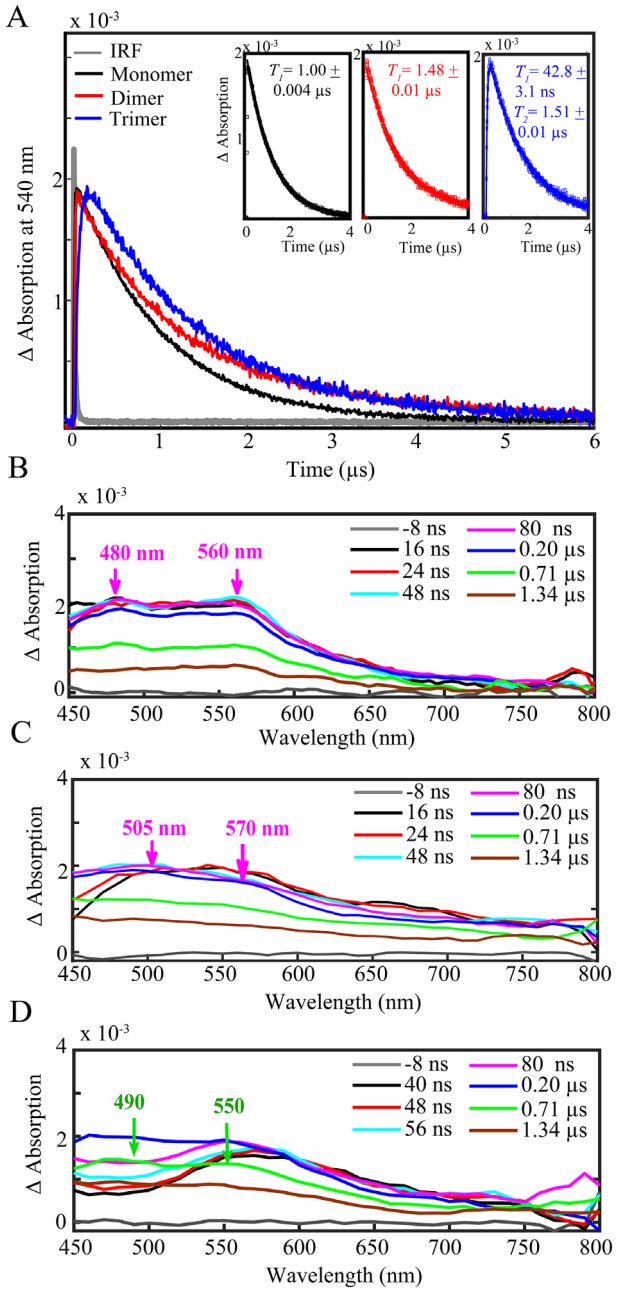

Figure 4. A) Global fit kinetic decay profiles at λ_{avg} from 480 to 560 nm after excitation at λ_{exc} = 355 nm illustrating the decay of the ^{3}ILCT for the Monomer (in black), Dimer (in red), and Trimer (in blue), as well as the ISC timeframe from the ^{1}ILCT to ^{3}ILCT for the Trimer fitted using a single exponential and double exponential function, respectively. The instrumental response function of 13 ns is shown in gray. OTA spectra of a solution of B) Monomer, C) Dimer D). Trimer dissolved in CH_3CN with an optical density of 0.3 at the pump excitation of 355 nm, at selected time intervals from 16–40 ns to 1.34 μs.

The global fit kinetics for the formation and decay of the ^{3}ILCT states were additionally probed in the nano-microsecond time scale (Figures 4A, S8). The formation of the ^{3}ILCT state for both the Monomer and Dimer occurs within the 13 ns IRF of the nanosecond OTA setup. The ^{3}ILCT state for the Monomer and Dimer further decays back to the ground state within time frames of 1.00 ± 0.004 μs and 1.48 ± 0.01 μs, respectively (Figure 4A, Table 2).

Table 2. Summary of the absorption wavelengths of the ^{1}ILCT and ^{3}ILCT excited states together with the kinetic lifetimes for the formation of the ILCT, ISC, and decay of the ^{3}ILCT states for the Monomer, Dimer, and Trimer. These results are based on the nano-microsecond OTA and pico-microsecond tr-XAS experiments illustrated in Figures 4 and 5.

Peak Absorption wavelengths of ^{1}IICT and ^{3}ILCT [nm]	^{1}ILCT state formation [fs]	ISC [ns]	^{3}ILCT state decay [μs]
Monomer ^{1}ILCT: 540 ^{3}ILCT: 480/560	235 ± 45	<13	1.00 ± 0.01
Dimer ^{1}ILCT: 570 ^{3}ILCT: 505/570	683 ± 174	<13	1.48 ± 0.01
Trimer ^{1}ILCT: 560 ^{3}ILCT: 490/550	730 ± 194	42.8 ± 3.1	1.51 ± 0.01

In contrast to the Monomer and Dimer, the ^{3}ILCT lifetime for the Trimer could be fitted to be 42.8 ± 3.1 ns, and additionally exhibited a slightly longer ^{3}ILCT decay lifetime of 1.51 ± 0.01 μs (Figure 4A, Table 2). The ISC rate of Dimeric Zn^{II} complexes with benzene 1,2-dithiolate ligands[29] and di(anisyl) amino substituents[30] have comparably been shown to exhibit ISC lifetimes of 10 and 25 ns, respectively. Similar to the femto-picosecond studies, nano-microsecond OTA shows increasing kinetic trends from the Monomer to the Dimer and the Trimer. This illustrates the importance of bulkier ligands in this family of Zn-based complexes, as they play a critical role in increasing the excited states´ stabilities and lifetimes. The metal centers in both the Dimer and Trimer also account for this increase, as their higher nuclearities and geometric arrangement allow for multiple interligand weak interactions, which tend to hamper structural distortion after photoexcitation.

2.3. Determination of the ^{3}ILCT State Through Pico-microsecond Time-resolved X-ray Spectroscopy

Following time-resolved optical measurements, tr-XAS with picosecond time resolution was employed to capture the electronic configurations of the excited states of the Monomer, Dimer, and Trimer. The complexes in solution were circulated through a stainless-steel nozzle into a free-flowing cylindrical jet inside an airtight aluminum chamber and pumped with a laser power of ~75 mW to avoid decomposition of the complexes to avoid decomposition of the complexes (Figure S9), and continuously degassed with nitrogen to prevent quenching of the ^{3}ILCT excited state (see Experimental Section for more details). The Zn complexes were optically pumped at 267 nm in the ligand-centered range and probed with X-ray pulses at different delays, from 80 ps to 20 μs (Figure S10). XANES spectra were collected at the Zn K-edge both before (laser off) and after (laser on) excitation (Figure 5, S11). A transient signal is obtained for each pump-probe delay to interrogate the photoinduced dynamics and electronic nature of the triplet excited states (Figures 5, S11).

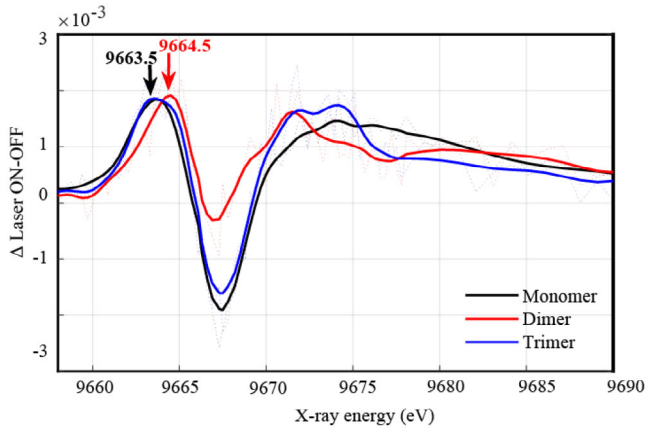

Figure 5. Time-resolved XAS spectra (laser ON-OFF) corresponding to the ^{3}ILCT state of 1 mM of the Monomer (black), Dimer (red), and Trimer (blue) at a delay of 306 ns between laser and X-ray pulses.

Figure 5 shows the time-resolved XANES spectrum at a time delay of 306 ns between the laser and X-ray pulses. A transient signal with a maximum peak energy of 9663.5–9664.5 eV together with a broad negative band between 9665 and 9670 eV is obtained (Figure 5), corresponding to the formation of the ^{3}ILCT state and ground state bleaching, respectively. Interestingly, the Monomer and Trimer display the transient signals with a maximum time-dependent energy of 9663.5 eV, whereas the Dimer shows a broader positive peak with the maximum at 9664.5 eV.

It should be mentioned that the excited state fractions of the photosensitizers between the laser pump excitation and X-ray probing were too low to reconstruct the EXAFS and structural conformations of the excited states. Upon comparing the LASER ON-OFF signal to other time-resolved studies[37d,48] conducted under similar experimental conditions, we expect to be forming less than 1% of the excited state. The structural differences between the ground and ^{3}ILCT states probed at the Zn K-edge are also very small (Table 1), as the transient signals are mainly due to a change of the electronic structures of the photosensitizers after photo-excitation. The Zn 1s orbitals of the ^{3}ILCT state move toward higher energies compared to the ground state, which is likely due to a change in the screening of the 3d electrons after ILCT electron transfer. This causes a negative energy shift in the Laser ON (^{3}ILCT state) versus the Laser OFF (ground state's) XANES signal upon photoexcitation (Figure 5). As a result, the LASER ON-OFF signal displays a transient feature with a positive and negative peak at lower and higher energies, respectively, as previously elaborated.

The gradual decay of the ^{3}ILCT transient signals from pico-microsecond tr-XAS studies was further analyzed by fixing the photon energies at 9663.5–9664.5 eV and varying the time delays between the laser and X-ray pulses (Figure S10). The Monomer, Dimer, and Trimer were shown to decay within 0.833 ± 0.310 μs, 1.44 ± 0.400 μs and 1.68 ± 0.300 μs, respectively (Figure S10), in agreement within the observed error bars with the nanosecond OTA results. The tr-XAS kinetic studies thus corroborate the formation of a ^{3}ILCT excited state, which is markedly longer-lived for the Trimer and Dimer versus the Monomer.

Table 3. DFT-optimized dihedral angles for the relative orientation of phenanthroline ligands bonded to a common Zn^{II} center. Geometries corresponding to the ground state and ^{3}ILCT state are compared.

		N-X-X dihedral angle [°]		
Complex	Zn^{II} coordination	Ground State	^{3}ILCT state	Difference
Monomer	$ZnN_4(ClO_4)$	66.7	80.7	14.0
Dimer	ZnN_4	69.1	67.2	1.9
	ZnN_4	69.0	68.6	0.4
Trimer	ZnN_4	70.1	70.0	0.1
	$ZnN_4(H_2O)(ClO_4)$	72.5	72.6	0.1
	ZnN_4 (H_2O)	67.1	67.4	0.3

It is important to remark that while the determinations of ^{3}ILCT states are possible through the time-resolved synchrotron-based XANES shown here, the femtosecond X-ray spectroscopic signature of the ^{1}ILCT states can in the future be determined at X-ray free electron lasers with time resolutions of tens of femtoseconds.[35] Furthermore, EXAFS of the ligand-centered excited states could not be determined at the K-edge energy probing the transition from the core 1s level to continuum[49] as the excited state corresponds to the formation of an intra-ligand charge transfer state. However, valence-to-core X-ray emission spectroscopy stemming from transitions from filled valence orbitals that are predominantly ligand in nature[50] to the Zn 1s core level could in the future provide additional insights into the identity of the ^{3}ILCT states upon photoexcitation.

2.4. Comparison of the Conformational Freedom Between the Ground and Excited States

As previously discussed, although the geometric changes between the triplet excited states and ground states are not dramatic (Table 1), the increased rigidity of the Dimer and Trimer with respect to the Monomer is evident when measuring the relative orientation of the phenanthroline planes for the singlet and triplet geometries as well as the changes in their torsional angles (Tables 1 and 3).

The dihedral angle between one nitrogen atom of one phenanthroline, the midpoint between the two nitrogen donors of the same ligand, the same midpoint in the opposing phenanthroline, and one of the donors in this second group (Figure 6) is first considered as a measure of the relative orientation of the phenanthroline ligands. Changes for this dihedral angle between the singlet and triplet optimized geometries are presented in Table 3. By far, the largest rearrangement occurs for the Monomer since the angle varies from 66.7° (singlet) to 80.7° (triplet) due to the large conformational freedom present in this complex as the two phenanthroline ligands are not chemically connected in this case. In contrast, the Dimer and Trimer are distorted by less than 2° since these complexes present a higher ligand strain associated with the ethyl and propyl ether bridging groups. Furthermore, weak interactions are favored in these

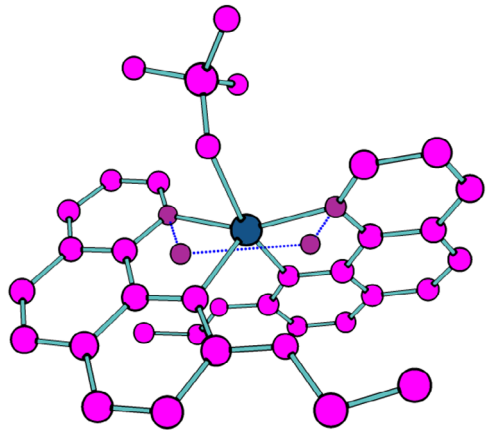

Figure 6. Scheme for the N-X-X-N dihedral. Positions involved in this angle are highlighted in dark gray and their connections are indicated by a dotted blue line. The Zn^{II} center and remaining atoms are depicted in purple and gray colors, respectively. Hydrogen atoms are omitted for clarity.

Table 4. Redox potentials recorded by cyclic voltammetry of the Monomer, Dimer, and Trimer in degassed CH_3CN versus Ag/AgCl, using 0.1 M $TBAPF_6$ as electrolyte and FcH/FcH^+ ($E^{Ox}{}_{\frac{1}{2}} = 0.46$ V) as the internal standard.

	Reduction [V]			Oxidation [V]	
Zn-Complex	$E^{Red3}{}_{1/2}$	$E^{Red2}{}_{1/2}$	$E^{Red1}{}_{1/2}$	$E^{Ox1}{}_{1/2}$	$E^{Ox1}{}_{1/2}$
Monomer	-	−1.16	−0.52	0.77	1.82
Dimer	–	−1.75	−0.61	1.01	1.43
Trimer	−1.45	−0.88	−0.68	0.82	1.67

two systems due to ligand arrangement, hence providing further rigidity to them.

2.5. Electrochemical Potentials of the Monomer, Dimer, and Trimer

Cyclic voltammetry was used for the determination of the electrochemical properties of the three Zn-based photosensitizers (Figure S12), and the potential values of all redox processes are listed in Table 4. The measurements were carried out using a two-electrode setup in freshly deoxygenated CH_3CN, using tetrabutylammonium hexafluorophosphate ($TBAPF_6$) as the electrolyte. Each Zn^{II} complex exhibited a few irreversible oxidations as well as reduction processes. Particularly two oxidative waves were recorded for all three complexes (0.77 and 1.82 V for the Monomer, 1.01 and 1.43 V for the Dimer, and 0.82 and 1.67 V for the Trimer) (Figure S12, Table 4). Additionally, both the Monomer and Dimer presented two reductions (-0.52 and -1.16 V, and -0.61 and -1.75 V for the Monomer and Dimer, respectively), while three reductive processes were observed in the case of the Trimer (-0.68, -0.88, and -1.45 V) (Figure S12, Table 4). The potential values of the first irreversible oxidations are located around 0.77, 1.01, and 0.82 V, and those of the first irreversible reduction waves at

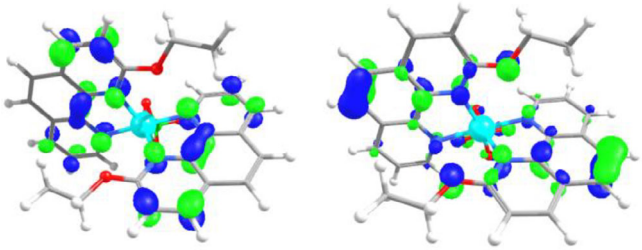

Figure 7. Molecular orbital corresponding to the unpaired electron for the reduction (left) and oxidation (right) processes for the Zn^{II} Monomer.

-0.52, -0.61, and -0.68 V versus Ag/AgCl for the Monomer, Dimer, and Trimer, respectively (Figure S12, Table 4).

DFT calculations for the oxidation and reduction processes of the Zn^{II} Monomer were further conducted. To have a reference of an analogous molecule exhibiting conventional MLCT transitions, we also calculated a copper(I) complex coordinated to two 2-etoxyphenantroline ligands with the same methodology. Finally, we repeated the calculations on the $[Ru(bpy)_3]^{2+}$ complex, since its electrochemical potentials for oxidation and reduction for both the ground and excited states are available in literature[51] and serve as a reference to check if our computational approach is accurate enough to describe these phenomena.[52]

Table S3 summarizes the DFT oxidation and reduction potentials for all calculated models. The agreement between experimental and DFT results for $[Ru(bpy)_3]^{2+}$ is adequate for our purposes. The ground state reduction potentials for all calculated complexes (Table S3) are similar, as the reduction is always centered in the phenanthroline or bipyridine ligands, which show comparable electron affinities. This point can be better visualized by plotting the molecular orbitals for the unpaired electron of the reduced species (Figure 7 for the Monomer, and S13-S14 for the remaining complexes). The Monomer displays a higher calculated oxidation potential compared to $[Cu(2\text{-EtOphen})_2]^+$ and $[Ru(bpy)_3]^{2+}$ (Figures S12, S13), as it is significantly harder to oxidize. Expectedly, the oxidation process is centered in the metal for $[Cu(2\text{-EtOphen})_2]^+$ and $[Ru(bpy)_3]^{2+}$ (Figures S12, S13) and in the ligand for the Zn^{II} Monomer (Figure 7). The difference between the reduction potentials of the ground and excited states for $[Ru(bpy)_3]^{2+}$ and the copper(I) complex is further less than that for the Zn^{II} Monomer, as the intraligand transitions are more energetic than MLCT (Table S3). Furthermore, the oxidation potential of the excited state of the Zn^{II} Monomer is higher and equal to -0.37 V compared to that for systems with MLCT transitions (-0.57 V and -0.85 V for the excited states of $[Ru(bpy)_3]^{2+}$ and $[Cu(2\text{-EtOphen})_2]^+$, respectively), but close enough to allow activity as an oxidant (Table S3).

3. Conclusion

We systematically elucidated the ground and excited states´ optical signatures, electronic configurations, and structures in three Zn^{II} photosensitizers with phenanthroline-derived ligands. A combination of experimental techniques, including

steady-state XAS, femto-microsecond OTA, and pico-microsecond tr-XAS which are further supported by TD-DFT calculations are employed.

Importantly, these results showed the formation of ^{1}ILCT states within femtosecond time scales followed by a nanosecond ISC process to generate ^{3}ILCT states, which decay back to the ground state within microseconds. Indeed, femto-picosecond OTA reveals the broad spectral absorption features of the ^{1}ILCT states, which are formed within 235 $\pm$ 45 fs, 683 $\pm$ 174 fs and 730 $\pm$ 194 fs for the Monomer, Dimer, and Trimer, respectively.

Nano-microsecond OTA further illustrates the formation of ^{3}ILCT states with broader absorption bands lying between 450 and 550 nm for the Zn photosensitizers, similar to that observed in the radical anion spectra of Cu complexes with analogous phenanthroline ligands.[47] Lastly, combined time-resolved OTA and tr-XAS show the ISC rates from the singlet to the triplet to occur within $<$13 ns for the Monomer and Dimer and within 42.8 $\pm$ 3.1 ns for the Trimer. The ^{3}ILCT states of the Monomer, Dimer, and Trimer were further confirmed from both XAS and optical methods to decay within increasing decay lifetimes of 1.00 $\pm$ 0.004 µs, 1.48 $\pm$ 0.01 and 1.51 $\pm$ 0.01 µs, respectively.

The Trimer and Dimer are hereby shown to display longer-lived singlet and triplet excited states relative to the Monomer, revealing the important role of steric hindrances exerted by their bulkier ligands in stabilizing their excited state conformations. These results outline the necessity to enhance the stabilities of Zn-based photosensitizers through ligand arrangements involving bimetallic and trimetallic helicates with adjacent aromatic ligands that can promote both π-π and CH-π interactions. As evidenced through both the dihedral and torsional angle calculations, the rearrangement from the ground to the ^{3}ILCT state decreases by increasing steric hinderances in the complexes, that is, Monomer $>$ Dimer $>$ Trimer.

These results are crucial toward identifying the critical factors influencing the structural reorganization of earth-abundant Zn-based photosensitizers in their excited states and can help control the energetics of the ^{1}ILCT and ^{3}ILCT decay rates. Furthermore, our current work offers guidelines toward the design of the next generation of improved Zn-based earth-abundant photosensitizers, bearing bulkier ligands, that could potentially be integrated into solar energy and artificial photosynthetic assemblies.

Supporting Information

The authors have cited additional references within the Supporting Information.[42–52]

Acknowledgments

D.M acknowledges funding from the Ramon y Cajal grant RYC2020-029863-I through the Instituto de Ciencia de Materiales de Madrid, Consejo Superior de Investigaciones Cientificas (CSIC-ICMM), PIE grant from CSIC-ICMM (20226AT001), and the Spanish Ministerio de Ciencia, Innovación y Universidades grants (PID2019-111086RA-I00, TED2021-1327 57B-I00, PID2022-143013OB-I00, CNS2023-145046). L.V acknowledges the Communidad de Madrid grant (PIPF-2022/ECO-25801) for a predoctoral fellowship. D.A. thanks FONDECYT Regular 1210325 project for financial support. Powered@NLHPC: This research was partially supported by the supercomputing infrastructure of the NLHPC (CCSS210001). P.L. thanks Fondecyt postdoctorado 3220267. L.L. thanks FONDECYT Regular 1231787. This research used resources of the Advanced Photon Source, a U.S. Department of Energy (DOE) Office of Science user facility operated for the DOE Office of Science by Argonne National Laboratory under Contract No. DE-AC02-06CH11357. S. G.-O. is grateful to the Spanish Ministry of Science and Innovation for a PhD grant (FPI, PRE2019-09345). V V.-M. acknowledges grants TED2021-131906A-100 and RYC2022-035200-I funded by Spanish Ministry of Science, Innovation and Universities (10.13039/501100011033) and support from the Regional Government of Madrid (2019-T2/IND-12737 and 2024-T1/TEC-31349). J C.-G. is grateful to the Spanish Ministry of Science and Innovation for projects PID2021-128313OB-I00 and PDC202-314587-1I00, and for a Research Consolidation Grant (CNS2022-36191). J.C.-G. also acknowledges funding from the Regional Government of Madrid through the NMAT2D-CM project. IMDEA Nanociencia acknowledges support by the 'Severo Ochoa' program for Centres of Excellence in R&D of the Spanish Ministry of Science and Innovation (CEX2020-001039-S).

Conflict of Interests

The authors declare no conflicts of interest.

Data Availability Statement

The data that support the findings of this study are available in the supplementary material of this article.

Keywords: earth-abundant Zn-based photosensitizers · excited-state structures · femto-microsecond optical transient absorption spectroscopy · Time-dependent Density Functional Theory · Time-resolved X-ray Spectroscopy

[1] A. Thapper, S. Styring, G. Saracco, W. Rutherford, B. Robert, A. Magnuson, W. Lubitz, A. Llobet, P. Kurz, A. Holzwarth, S. Fiechter, H. d. Grott, S. Campagna, A. Braun, H. Bercegol, V. Artero, *Green* **2010**, *3*, 43.
[2] R. L. House, N. Y. M. Iha, R. L. Coppo, L. Alibabaei, B. D. Sherman, P. Kang, M. K. Brennaman, P. G. Hoertz, T. J. Meyer, *J. PhotoChem. PhotoBiol. C: PhotoChem. Rev.* **2015**, *25*, 32.
[3] C. Herrero, A. Quaranta, W. Leibl, A. W. Rutherford, A. Aukauloo, *Energy Environ.Sci* **2011**, *4*, 2353.
[4] a) A. Juris, V. Balzani, P. Belser, A. von Zelewsky, *Helv.Chim.Acta* **1981**, *64*, 2175; b) C. R. Bock, J. A. Connor, A. R. Gutierrez, T. J. Meyer, D. G. Whitten, B. P. Sullivan, J. K. Nagle, *J. Am. Chem. Soc.* **1979**, *101*, 4815; c) M. Kirch, J. M. Lehn, J. P. J. H. C. A. Sauvage, *Helv.Chim.Acta* **1979**, *62*, 1345; d) C. R. Bock, J. A. Connor, A. R. Gutierrez, T. J. Meyer, D. G. Whitten, B. P. Sullivan, J. K. Nagle, *Chem.Phys. Lett.* **1979**, *61*, 522.
[5] B. Probst, C. Kolano, P. Hamm, R. Alberto, *Inorg. Chem.* **2009**, *48*, 1836.
[6] a) M. Irikura, Y. Tamaki, O. Ishitani, *Chem.Sci.* **2021**, *12*, 13888; b) Y. Tamaki, K. Koike, O. Ishitani, *Chem.Sci* **2015**, *6*, 7213.

[7] a) D. R. Whang, K. Sakai, S. Y. Park, *Angew. Chem., Int. Ed.* **2013**, *52*, 11612; b) F. Gärtner, B. Sundararaju, A.-E. Surkus, A. Boddien, B. Loges, H. Junge, P. H. Dixneuf, M. Beller, *Angew.Chem.Int.Ed* **2009**, *48*, 9962; c) D. Hollmann, F. Gärtner, R. Ludwig, E. Barsch, H. Junge, M. Blug, S. Hoch, M. Beller, A. Brückner, *Angew.Chem.Int.Ed* **2011**, *50*, 10246; d) F. Gärtner, A. Boddien, E. Barsch, K. Fumino, S. Losse, H. Junge, D. Hollmann, A. Brückner, R. Ludwig, M. Beller, *Chem. Eur. J.* **2011**, *17*, 6425; e) P. Zhang, M. Wang, Y. Na, X. Li, Y. Jiang, L. Sun, *Dalton Trans.* **2010**, *39*, 1204.

[8] a) J. Kiwi, M. Graetzel, *J. Am. Chem. Soc.* **1979**, *101*, 7214; b) X. Wang, S. Goeb, Z. Ji, N. A. Pogulaichenko, F. N. Castellano, *Inorg. Chem.* **2011**, *50*, 705; c) P. Du, J. Schneider, G. Luo, W. W. Brennessel, R. Eisenberg, *Inorg.Chem* **2009**, *48*, 4952.

[9] C. Wegeberg, O. S. Wenger, *JACS Au.* **2021**, *1*, 1860.

[10] D. Moonshiram, P. Garrido-Barros, C. Gimbert-Suriñach, A. Picón, C. Liu, X. Zhang, M. Karnahl, A. Llobet, *Chem.Eur. J.* **2018**, *24*, 6464.

[11] L. Velasco, L. Llanos, P. Levín, A. Vega, J. Yu, X. Zhang, L. Lemus, D. Aravena, D. Moonshiram, *Phys.Chem.Chem.Phys* **2021**, *23*, 3656.

[12] S. Shi, M. C. Jung, C. Coburn, A. Tadle, D. Sylvinson M R, P. I. Djurovich, S. R. Forrest, M. E. Thompson, *J.Am.Chem.Soc* **2019**, *141*, 3576.

[13] J. B. Bilger, C. Kerzig, C. B. Larsen, O. S. Wenger, *J.Am.Chem.Soc* **2021**, *143*, 1651.

[14] L. A. Büldt, X. Guo, R. Vogel, A. Prescimone, O. S. Wenger, *J.Am.Chem.Soc* **2017**, *139*, 985.

[15] C. Wegeberg, D. Häussinger, O. S. Wenger, *J.Am.Chem.Soc* **2021**, *143*, 15800.

[16] S. Treiling, C. Wang, C. Förster, F. Reichenauer, J. Kalmbach, P. Boden, J. P. Harris, L. M. Carrella, E. Rentschler, U. Resch-Genger, C. Reber, M. Seitz, M. Gerhards, K. Heinze, *Nat.Chem* **2019**, *58*, 18075.

[17] J.-R. Jiménez, M. Poncet, B. Doistau, C. Besnard, C. Piguet, *Dalton Trans.* **2020**, *49*, 13528.

[18] P. Herr, C. Kerzig, C. B. Larsen, D. Häussinger, O. S. Wenger, *Nat. Chem.* **2021**, *13*, 956.

[19] J. P. Harris, C. Reber, H. E. Colmer, T. A. Jackson, A. P. Forshaw, J. M. Smith, R. A. Kinney, J. Telser, *Can.J.Chem* **2017**, *95*, 547.

[20] J. Steube, A. Kruse, O. S. Bokareva, T. Reuter, S. Demeshko, R. Schoch, M. A. Argüello Cordero, A. Krishna, S. Hohloch, F. Meyer, K. Heinze, O. Kühn, S. Lochbrunner, M. Bauer, *Nat.Chem* **2023**, *15*, 468.

[21] P. Chábera, Y. Liu, O. Prakash, E. Thyrhaug, A. E. Nahhas, A. Honarfar, S. Essén, L. A. Fredin, T. C. B. Harlang, K. S. Kjær, K. Handrup, F. Ericson, H. Tatsuno, K. Morgan, J. Schnadt, L. Häggström, T. Ericsson, A. Sobkowiak, S. Lidin, P. Huang, S. Styring, J. Uhlig, J. Bendix, R. Lomoth, V. Sundström, P. Persson, K. Wärnmark, *Nature* **2017**, *543*, 695.

[22] J. D. Cope, J. A. Denny, R. W. Lamb, L. E. McNamara, N. I. Hammer, C. E. Webster, T. K. Hollis, *J.Org.Chem* **2017**, *845*, 258.

[23] Y.-S. Wong, M.-C. Tang, M. Ng, V. W.-W. Yam, *J.Am.Chem.Soc* **2020**, *142*, 7638.

[24] S. Kaufhold, N. W. Rosemann, P. Chábera, L. Lindh, I. Bolaño Losada, J. Uhlig, T. Pascher, D. Strand, K. Wärnmark, A. Yartsev, P. Persson, *J.Am.Chem.Soc* **2021**, *143*, 1307.

[25] a) M. Dorn, J. Kalmbach, P. Boden, A. Päpcke, S. Gómez, C. Förster, F. Kuczelinis, L. M. Carrella, L. A. Büldt, N. H. Bings, E. Rentschler, S. Lochbrunner, L. González, M. Gerhards, M. Seitz, K. Heinze, *J. Am. Chem. Soc.* **2020**, *142*, 7947; b) M. Dorn, J. Kalmbach, P. Boden, A. Kruse, C. Dab, C. Reber, G. Niedner-Schatteburg, S. Lochbrunner, M. Gerhards, M. Seitz, K. Heinze, *Chem.Sci* **2021**, *12*, 10780.

[26] a) R. Tabone, D. Feser, E. D. Lemma, U. Schepers, C. Bizzarri, *Front.Chem* **2021**, *9*, 754420; b) M. A. Filatov, A. Y. Lebedev, S. N. Mukhin, S. A. Vinogradov, A. V. Cheprakov, *J.Am.Chem.Soc* **2010**, *132*, 9552; c) G. Yu, S. Yin, Y. Liu, Z. Shuai, D. Zhu, *J. Am. Chem. Soc.* **2003**, *125*, 14816; d) S. M. Borisov, R. Pommer, J. Svec, S. Peters, V. Novakova, I. Klimant, *J.Mater.Chem.C. 2018*, 8999.

[27] K. S. Kjær, N. Kaul, O. Prakash, P. Chábera, N. W. Rosemann, A. Honarfar, O. Gordivska, L. A. Fredin, K.-E. Bergquist, L. Häggström, T. Ericsson, L. Lindh, A. Yartsev, S. Styring, P. Huang, J. Uhlig, J. Bendix, D. Strand, V. Sundström, P. Persson, R. Lomoth, K. Wärnmark, *Science* **2019**, *363*, 249.

[28] A. K. Pal, C. Li, G. S. Hanan, E. Zysman-Colman, *Angew.Chem.Int.Ed* **2018**, *57*, 8027.

[29] O. Mrózek, M. Mitra, B. Hupp, A. Belyaev, N. Lüdtke, D. Wagner, C. Wang, O. S. Wenger, C. M. Marian, A. Steffen, *Chem.Eur.J.* **2023**, *29*, e202203980.

[30] J. A. Kübler, B. Pfund, O. S. Wenger, *JACS Au* **2022**, *2*, 2367.

[31] P. Levín, D. Escudero, N. Díaz, A. Oliver, A. G. Lappin, G. Ferraudi, L. Lemus, *Inorg. Chem.* **2020**, *59*, 1660.

[32] M. Schmittel, A. Ganz, *Chem.Comm* **1997**, 999.

[33] G. Consiglio, I. P. Oliveri, S. Cacciola, G. Maccarrone, S. Failla, S. Di Bella, *Dalton Trans.* **2020**, *49*, 5121.

[34] a) N. Sinha, O. S. Wenger, *J. Am. Chem. Soc.* **2023**, *145*, 4903; b) M. Schmittel, A. Ganz, D. Fenske, M. Herderich, *J.Chem.Soc.Dalton. Trans.* **2000**, 353.

[35] L. X. Chen, X. Zhang, *J.Phys.Chem.Lett* **2013**, *4*, 4000.

[36] K. J. Gaffney, *Chem.Sci* **2021**, *12*, 8010.

[37] a) M. Chergui, *Struct.Dyn* **2016**, 031001; b) M. Chergui, E. Collet, *Chem.Rev* **2017**, *117*, 11025; c) L. Velasco, C. Liu, X. Zhang, S. Grau, M. Gil-Sepulcre, C. Gimbert-Suriñach, A. Picón, A. Llobet, S. DeBeer, D. Moonshiram, *ChemSusChem* **2023**, *16*, e202300719; d) J.-W. Wang, X. Zhang, L. Velasco, M. Karnahl, Z. Li, Z.-M. Luo, Y. Huang, J. Yu, W. Hu, X. Zhang, K. Yamauchi, K. Sakai, D. Moonshiram, G. Ouyang, *JACS Au* **2023**, *3*, 1984; e) S. Iglesias, A. Gamonal, A. Abudulimu, A. Picón, E. Carrasco, D. Écija, C. Liu, L. Luer, X. Zhang, J. S. Costa, D. Moonshiram, *Chem. Eur. J* **2020**, *26*, 10801; f) M. Rentschler, S. Iglesias, M.-A. Schmid, C. Liu, S. Tschierlei, W. Frey, X. Zhang, M. Karnahl, D. Moonshiram, *Chem. Eur. J* **2020**, *26*, 9527; g) P. Gotico, D. Moonshiram, C. Liu, X. Zhang, R. Guillot, A. Quaranta, Z. Halime, W. Leibl, A. Aukauloo, *Chem. Eur. J* **2020**, *26*, 2859; h) D. Moonshiram, A. Picón, A. Vazquez-Mayagoitia, X. Zhang, M.-F. Tu, P. Garrido-Barros, J.-P. Mahy, F. Avenier, A. Aukauloo, *Chem.Comm* **2017**, *53*, 2725; i) D. Moonshiram, A. Guda, L. Kohler, A. Picon, S. Guda, C. S. Lehmann, X. Zhang, S. H. Southworth, K. L. Mulfort, *J.Phys.Chem.C* **2016**, *120*, 20049; j) D. Moonshiram, C. Gimbert-Suriñach, A. Guda, A. Picon, C. S. Lehmann, X. Zhang, G. Doumy, A. M. March, J. Benet-Buchholz, A. Soldatov, A. Llobet, S. H. Southworth, *J.Am.Chem.Soc* **2016**, *138*, 10586.

[38] N. Z. Alqahtani, T. G. Blevins, C. E. McCusker, *J.Phys.Chem.A* **2019**, *123*, 10011.

[39] a) J. W. Furness, A. D. Kaplan, J. Ning, J. P. Perdew, J. Sun, *J.Phys.Chem.Lett* **2020**, *11*, 8208; b) J. W. Furness, A. D. Kaplan, J. Ning, J. P. Perdew, J. Sun, *J.Phys.Chem.Lett* **2020**, *11*, 9248.

[40] A. V. Marenich, C. J. Cramer, D. G. Truhlar, *J.Phys.Chem.B* **2009**, *113*, 6378.

[41] R. Sarangi, *Coord.Chem.Rev* **2013**, *257*, 459.

[42] a) D. E. Díaz, L. Llanos, P. Arce, R. Lorca, J. Guerrero, J. Costamagna, D. Aravena, G. Ferraudi, A. Oliver, A. G. Lappin, L. Lemus, *Chem. Eur. J.* **2018**, *24*, 13839; b) L. Lemus, J. Guerrero, J. Costamagna, G. Estiu, G. Ferraudi, A. G. Lappin, A. Oliver, B. C. Noll, *Inorg.Chem* **2010**, *49*, 4023.

[43] S. Hirata, M. Head-Gordon, *Chem.Phys.Lett* **1999**, *314*, 291.

[44] J.-D. Chai, M. Head-Gordon, *J.Chem.Phys* **2008**, 128.

[45] Y.-S. Lin, G.-D. Li, S.-P. Mao, J.-D. Chai, *J.Chem.Theory.Comput* **2013**, *9*, 263.

[46] J. Savolainen, D. van der Linden, N. Dijkhuizen, J. L. Herek, *J.PhotoChem.PhotoBiol.A: Chem* **2008**, *196*, 99.

[47] L. Kohler, R. G. Hadt, D. Hayes, L. X. Chen, K. L. Mulfort, *Dalton Trans.* **2017**, *46*, 13088.

[48] M. Sauvan, A. Ugale, L. Velasco, A. Charisiadis, F. Ma, X. Zhang, J.-W. Wang, D. Moonshiram, *Chem.Comm* **2025**, *61*, 4788.

[49] J. Yano, V. K. Yachandra, *Photosynth. Res.* **2009**, *102*, 241.

[50] C. Roemelt, S. Peredkov, F. Neese, M. Roemelt, S. DeBeer, *Phys.Chem.Chem.Phys* **2024**, *26*, 19960.

[51] A. Juris, V. Balzani, F. Barigelletti, S. Campagna, P. Belser, A. von Zelewsky, *Coord.Chem.Rev* **1988**, *84*, 85.

[52] E. Medina, B. Pinter, *Catalysts* **2020**, *10*, 80.

Manuscript received: May 12, 2025
Revised manuscript received: June 12, 2025
Version of record online: August 1, 2025